

Look, Remember and Reason: Visual Reasoning with Grounded Rationales

Apratim Bhattacharyya¹ Sunny Panchal¹ Mingu Lee¹ Reza Pourreza¹ Pulkit Madan¹ Roland Memisevic¹

Abstract

Large language models have recently shown human level performance on a variety of reasoning tasks. However, the ability of these models to perform complex visual reasoning has not been studied in detail yet. A key challenge in many visual reasoning tasks is that the visual information needs to be tightly integrated in the reasoning process. We propose to address this challenge by drawing inspiration from human visual problem solving which depends on a variety of low-level visual capabilities. It can often be cast as the three step-process of “Look, Remember, Reason”: visual information is incrementally extracted using low-level visual routines in a step-by-step fashion until a final answer is reached. We follow the same paradigm to enable existing large language models, with minimal changes to the architecture, to solve visual reasoning problems. To this end, we introduce rationales over the visual input that allow us to integrate low-level visual capabilities, such as object recognition and tracking, as surrogate tasks. We show competitive performance on diverse visual reasoning tasks from the CLEVR, CATER, and ACRE datasets over state-of-the-art models designed specifically for these tasks.

1. Introduction

Autoregressive large language models (LLMs) have shown impressive results on various reasoning tasks such as on grade school math problems (Cobbe et al., 2021) and even on LSAT (OpenAI, 2023). Language models designed for these problems process only textual data to reason and solve the target task. Many real-world scenarios, however, require humans to reason in complex domains that engage various heterogeneous sensory inputs, *e.g.*, perceptual cues and language. Motivated by this, multimodal LLMs (Alayrac et al., 2022; Koh et al., 2023; Zhang et al., 2023b) have gained

^{*}Equal contribution ¹Qualcomm AI Research, an initiative of Qualcomm Technologies, Inc.. Correspondence to: Apratim Bhattacharyya <aprabhat@qti.qualcomm.com>.



Figure 1. Our “Look, Remember, Reason” (LRR) model solves complex visual reasoning problems by generating grounded rationales. Crucially, we train the model on surrogate tasks, *e.g.*, object re-identification, to enable necessary low-level visual capabilities. Our model “looks” at the visual input to extract relevant low-level information step-by-step, and it “remembers” results of intermediate steps. In the above example, this allows our LRR model to “reason” whether the query objects could activate the “Blicket” machine.

traction, which model information both from the textual and the visual domains. While these models perform well on the tasks that rely on the global visual-textual relationships, *e.g.*, captioning or dialogue (Alayrac et al., 2022; Driess et al., 2023; Koh et al., 2023), the ability of multimodal LLMs to understand spatio-temporal relationships and causal structures in visual data is rather under-explored. It is unclear to what degree the recent success of such models on visual reasoning is due to the models’ encyclopedic common sense knowledge or their ability to perform complex visual perception. Disentangling high-level reasoning and background knowledge from perceptual capabilities is crucial to better understand and improve the visual reasoning capabilities of these models. Therefore, in this work, we focus on visual reasoning problems (Girdhar & Ramanan, 2020; Johnson et al., 2017; Zhang et al., 2021) which do not require ex-

tensive common sense or background knowledge and are without the implicit biases over the scene and the object structure.

Consider the visual reasoning problem such as in Figure 1 from ACRE (Zhang et al., 2021), where the objective is to correctly answer whether the query objects (in bottom left) would activate the “Blicket” machine. Humans can solve this problem through a multi-step reasoning process where we attend to and extract visual information step by step using our low-level visual capabilities, such as object recognition and re-identification. For example, one strategy that humans may follow to solve this problem is: read the question; inspect the scene to create an overview of the present objects as well as any relevant low-level visual information; memorize the relevant information along the way; finally state the answer based on the extracted information. Such a reasoning process is crucial to deal with both the complexity of the task and the need to filter the rich visual data for relevant information. In short, such a reasoning process can be thought of as consisting of the three intermediate sub-tasks “Look, Remember, Reason” – looking for relevant visual cues, remembering the relevant cues along the way, and finally aggregating the collected information to arrive at the final answer. In this work, we boost the uni-modal large language models for texts to perform general-purpose multi-modal visual reasoning by augmenting them with *low-level visual capabilities*.

Our key contributions are: 1. We equip an off-the-shelf language model with the low-level visual capabilities to solve a diverse range of visual reasoning tasks. This is accomplished by training the LLM indirectly using surrogate tasks expressed in natural language requiring the generation of relevant rationales that follow the paradigm of “Look, Remember, Reason” and are grounded in the visual input. 2. We show that it is crucial in these tasks to let high-level concepts modulate the perceptual pathway, and we present an adapter module that accomplishes this through top-down attention controlled by the LLM. 3. Our general-purpose LRR model can perform varied visual reasoning tasks, including spatial reasoning (CLEVR;(Johnson et al., 2017)), temporal reasoning (CATER;(Girdhar & Ramanan, 2020)), and causal visual reasoning (ACRE;(Zhang et al., 2021)). Our approach outperforms prior state-of-the-art particularly designed to perform one of these tasks by a large margin.

2. Related Work

Large language models and reasoning. Large language models have shown strong performance on a variety of natural language processing tasks, *e.g.*, question answering, translation, summarization (Brown et al., 2020; Raffel et al., 2019). This progress has been enabled by scaling model size (Chowdhery et al., 2022; Kaplan et al., 2020;

Rae et al., 2021), which has enhanced models’ ability to learn in-context and unlock “emergent abilities” such as the ability to perform well on very challenging reasoning tasks (d’Avila Garcez & Lamb, 2020; Marcus, 2018; 2020) like commonsense reasoning (Wei et al., 2021; Sanh et al., 2022), symbolic reasoning (Ichler et al., 2022; Yao et al., 2022) and mathematical reasoning (Lewkowycz et al., 2022). The progress in reasoning abilities has been fueled by “chain-of-thought” or “rationale” based methods which aim to mimic human reasoning processes. This has been successfully applied to improve performance on arithmetic programs (Ling et al., 2017), and commonsense reasoning (Rajani et al., 2019) among others. LLMs can learn multi-step tasks like long-division (Recchia, 2021) through rationales and manipulation of an external environment in the form of a “scratch paper”. Similarly, Nye et al. (2021) outputs intermediate steps to improve performance on computational problems. More recently, by utilizing models with a strong ability to learn in context, the possibility of generating rationales through prompting has been demonstrated in Kojima et al. (2022); Wei et al. (2022b). Further, producing multiple chains of thought and selecting the final answer by majority vote has shown promise in Wang et al. (2022); Wei et al. (2022b). In this work, we aim to leverage the abilities of LLMs to reason in natural language by generating rationales and performing visual reasoning tasks.

Multi-modal language models. Analogous to the large-scale models for text, there have been breakthroughs in the development of large multimodal approaches which can deal with multi-modal, specifically visual, inputs in addition to the text. Pix2seq (Chen et al., 2022) utilize auto-regressive language models to extract low-level visual information from images. ViperGPT (Surís et al., 2023), VisProg (Gupta & Kembhavi, 2022) and Chameleon (Lu et al., 2023) use language-based LLMs with vision sub-modules for multi-modal tasks. Other approaches focus on joint modeling of visual and textual data. Such models include the CLIP (Radford et al., 2021) and BLIP (Li et al., 2022) which utilize natural language instead of image-level class labels. Flamingo (Alayrac et al., 2022) introduces a family of language and vision models which are pre-trained on diverse vision and language tasks with a large amount of vision and text data available from the web. Recent approaches such as CM3 (Aghajanyan et al., 2022) train a multimodal LLM on a large HTML corpus for image and text generation. Other approaches Eichenberg et al. (2022); Li et al. (2023); Liu et al. (2023); Mañas et al. (2023); Tsimpoukelli et al. (2021), instead of training vision and language models from scratch on the multimodal data, incorporate pretrained LLMs as language priors. Methods like Frozen (Tsimpoukelli et al., 2021), leverage pretrained LLMs and train a vision encoder to encode images as a sequence of tokens which can be presented to the transformer in the same form as the text.

PaLM-E (Driess et al., 2023) provides images and text as interleaved multimodal latent vectors, allowing the model to process multiple images within any part of a sentence which serves as an input to the LLM where the model is trained end-to-end. LLaMA-Adapter (Zhang et al., 2023a) introduces a adapter layer with zero-init attention to enable multimodal inputs with the LLaMA model (Touvron et al., 2023). LLaVA (Liu et al., 2023) finetunes the LLaMA model which is presented with the output of the vision encoder obtained from conversational data. A low-rank adaption to finetune a LLaMA model in a setting similar to LLaVA is further explored in mPLUG-owl (Ye et al., 2023). FROMAGe (Koh et al., 2023) on the other hand, freezes the language model, and fine-tunes the input and output linear layers to encode multimodal interactions. In our work, we systematically study the role of low-level visual skills for visual reasoning and introduce rationales with corresponding surrogate tasks.

Attention-based models and visual reasoning. Attention-based models have been studied extensively for visual reasoning (Ding et al., 2021; Hu et al., 2017; Hudson & Manning, 2018; Kamath et al., 2021; Mahajan & Roth, 2020; Santoro et al., 2017). Recent advances include an object-centric encoder and a transformer reasoning module to solve RPM-like benchmarks (Mondal et al., 2023), multi-hop feature modulation (Strub et al., 2018) and cascaded modulation networks (Yao et al., 2018) that use a multi-step comprehension process, neural interpreters (Rahaman et al., 2021) that factorize inference in a self-attention network and ALANS learner (Zhang et al., 2022a) that combines abstract algebra and representation theory. Calibrating concepts and operations (Li et al., 2021) enables neural symbolic models to capture underlying data characteristics and perform hierarchical inference. In contrast to these approaches with task-specific architectures, we focus on using off-the-shelf LLMs with spatial features from a CNN for visual reasoning. We instill the ability to extract object-centric information in the network by using rationales, instead of resorting to specialized object detection modules.

3. Look, Remember, Reason

To allow visual reasoning by exploiting the highly expressive large language models, we propose a novel “*Look, Remember, Reason*” framework. Our LRR model is based on a pre-trained LLM backbone, with additional cross attention layers (Dou et al., 2022; Rahman et al., 2023; Vaswani et al., 2017) to enable multi-modal inputs. To address the challenges presented by visual reasoning problems, we propose rationales obtained from multimodal signals. Unlike prior work (Zhang et al., 2023a;b), our rationales additionally include low-level visual surrogate tasks expressed in natural language crucial for visual reasoning tasks. These are supported by a top-down attention mechanism that allows

high-level concepts to modulate the perceptual pathway. In the following, we first describe our LRR approach, followed by our rationales.

3.1. Auto-regressive Pipeline

Inspired by the success of auto-regressive models in reasoning tasks (Cobbe et al., 2021), we formalize our LRR model in the auto-regressive framework. Our LRR model (depicted in Figure 2) with parameters θ receives an interleaved stream of visual input, $\mathbf{I} = (\mathbf{v}_1, \dots, \mathbf{v}_{t_v})$, e.g., an image or a sequence of video frames of length t_v , along with (tokenized) text $\mathbf{S} = (\mathbf{s}_1, \dots, \mathbf{s}_{t_s})$ of length t_s . The tokenized text includes the rationales and answers to visual reasoning problems. We train the model by maximizing log-likelihood of the next token given the interleaved sequence of previous tokens and images,

$$\log(p_{\theta}(\mathbf{S})) = \sum_{t'_s} \log(\mathbf{s}_{t'_s} | \mathbf{s}_1, \dots, \mathbf{s}_{t'_s-1}, \mathbf{v}_1, \dots, \mathbf{v}_{t'_v}) \quad (1)$$

where, $(\mathbf{v}_1, \dots, \mathbf{v}_{t'_v})$ is the interleaved visual input sequence upto the text token $\mathbf{s}_{t'_s}$. The backbone of our model consists of an off-the-shelf LLM. We use models from the OPT family (Zhang et al., 2022b), but verified that similar performance can be achieved using other pre-trained models (Gao et al., 2021; Scao et al., 2022). The parameters are initialized from pre-trained LLMs, which allows us to exploit their existing reasoning capabilities. While the LLMs we use as backbone are trained on text only, visual reasoning relies on the extraction of visual information about spatial and temporal relationships between objects in the scene. Therefore, in our multi-modal setup, visual information \mathbf{I} needs to be mapped to the text-based representation space of the LLM. The key challenge here is that in comparison to text tokens, images are highly information dense – reflected in the popular adage “An image is worth a thousand words”.

State-of-the-art multi-modal LLMs (Alayrac et al., 2022; Koh et al., 2023) map visual information to the textual domain using specially trained visual encoders such as Perceiver (Jaegle et al., 2021) or CLIP (Radford et al., 2021). As such visual encoders are trained to capture high-level global semantics, they are not well suited to capture low-level visual information underlying complex reasoning tasks. Models like PaLM-E (Driess et al., 2023) map visual information from image patches directly to the input token space of an LLM using a ViT or OSRT model (Dosovitskiy et al., 2021; Sajjadi et al., 2022). It is challenging to capture the relevant visual information with the prior approaches due to the aforementioned discrepancy between the information density of images and text tokens. Therefore, we propose to use low-level grid-level visual features from an off-the-shelf CNN which preserves low-level visual information, coupled with a top-down attention mechanism that allows the LLM to directly extract low-level visual information.

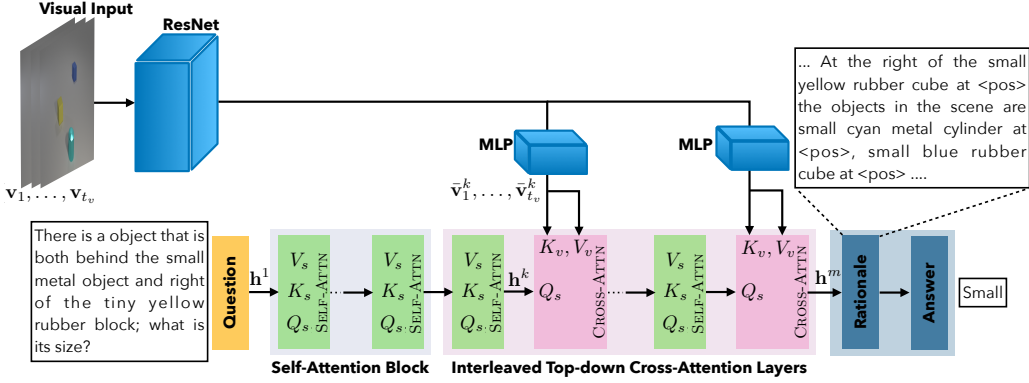


Figure 2. The architecture of our LRR model, highlighting the use of interleaved top-down cross-attention layers in between self-attention layers higher up in the hierarchy.

3.2. Top-down Cross Attention

Our top-down attention mechanism exploits the rich hierarchical representation encoded in the hidden states $\mathbf{h} = \{\mathbf{h}^1, \dots, \mathbf{h}^m\}$ of the LLM, where m is the number of self-attention layers in the LLM and $\mathbf{h}^i \in \mathbb{R}^{t \times q}$. Here, t is sequence length $t = t_v + t_s$ and q is the dimensionality of the embedding space. The first embedding layer of the LLM encodes tokens, whereas subsequent layers contain progressively richer and more information-dense representations than encode increasingly global information. Therefore, we propose to use the embedding layers higher in the hierarchy in our top-down attention mechanism to guide the information extraction process from visual inputs.

Our LRR model, as shown in Figure 2, employs grid-level visual features obtained from ResNet(He et al., 2016) based CNN, which allows us to preserve spatial information crucial for visual reasoning tasks. The adoption of a simple CNN ensures that our model is applicable across a variety of visual reasoning problems. In our approach, the CNN encodes the input image sequence $\mathbf{I} = (\mathbf{v}_1, \dots, \mathbf{v}_{t_v})$ into $\bar{\mathbf{I}} = (\bar{\mathbf{v}}_1, \dots, \bar{\mathbf{v}}_{t_v})$, where $\bar{\mathbf{v}}_i = \text{CNN}(\mathbf{v}_i)$ and $\bar{\mathbf{v}}_i \in \mathbb{R}^{g \times q'}$. Here, g is the size of the grid and q' the dimensionality of the CNN embedding space.

To integrate and “look” for the visual information from the CNN in our LLM pipeline, we employ cross attention (CROSS-ATTN) layers at higher levels $\{k, \dots, m\}$ of the hierarchical LLM representation space, in addition to the self-attention (SELF-ATTN) layers present in the backbone LLM (c.f. Figure 2). The grid level features $\bar{\mathbf{I}}$ are first transformed using a multi-layer perceptron (MLP) for every cross-attention layer. For example, we learn a mapping $\text{MLP}_k : \mathbb{R}^{q'} \rightarrow \mathbb{R}^q$ to transform the grid level features $\bar{\mathbf{v}}_i$ as $\hat{\mathbf{v}}_i^k = \text{MLP}_k(\bar{\mathbf{v}}_i)$, for use as input to the first top-down cross attention layer. Furthermore, to preserve spatial information, we concatenate positional embeddings to each grid element $\hat{\mathbf{v}}_i^k$. The grid level image features $\hat{\mathbf{v}}_i^k$ fused with positional embeddings allow for top-down attention where the LLM guides the information extraction process

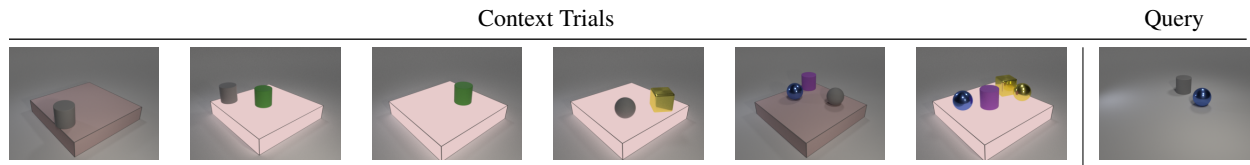
using the representation \mathbf{h}^k . We use the representation $\hat{\mathbf{h}}^k$ after the application of the self-attention layer to guide the visual feature extraction process in the cross-attention layer. From Figure 2, the hidden representation $\hat{\mathbf{h}}^k$ is transformed by a linear projection to serve as the query vector (Q_s) and the visual features $\hat{\mathbf{v}}_i^k$ are linearly transformed to the keys and values (K_v, V_v) of the cross attention layer respectively,

$$\begin{aligned} \hat{\mathbf{h}}^k &= \text{SELF-ATTN}(\mathbf{h}^k) \\ \hat{\mathbf{v}}_i^k &= \text{CROSS-ATTN}(\hat{\mathbf{h}}^k, \hat{\mathbf{v}}_i^k) \\ \mathbf{h}^{k+1} &= \mathbf{h}^k + \hat{\mathbf{h}}^k + \hat{\mathbf{v}}_i^k \\ \mathbf{h}^{k+1} &= \text{FFN}(\mathbf{h}^{k+1}) + \mathbf{h}^{k+1} \end{aligned} \quad (2)$$

where FFN denotes a feedforward layer defined the same way as in (Vaswani et al., 2017). We use the hidden state $\hat{\mathbf{h}}^i$ as a query vector that encodes global semantics in the cross-attention layers with the spatial grid features $\hat{\mathbf{v}}_i^k$ as keys and values. This allows the LLM to extract information relevant to solving visual reasoning problems, including object locations and their spatial relationships in $\hat{\mathbf{v}}_i^k$. The hidden representation at level $k+1$ now includes information from both the textual ($\hat{\mathbf{h}}^k$) and visual domains ($\hat{\mathbf{v}}_i^k$) and is thus multi-modal and includes low-level visual information. This is instrumental in generating rationales for visual reasoning tasks as discussed in the following.

3.3. Rationales with Surrogate Tasks

Many complex reasoning tasks including visual reasoning, have serial step-by-step solutions, i.e., rationales, expressible in natural language (c.f. Figure 1). This property can be exploited in pure text-based reasoning tasks by placing exemplary rationales (“chain-of-thought”) as a prompt to the LLM along with the statement of the task to be solved (e.g., (Wei et al., 2022a)). However, this method of prompting with exemplary rationales cannot be used directly for visual reasoning as many of these tasks additionally rely on a number of generic, low-level visual skills. Examples of such visual skills include the ability to detect, describe



Rationale: The task is to detect whether the following combination of objects activate the blicket machine, which activates when we put a blicket on it. Next, we will conduct six trials where we put a combination of objects on the machine. Trial 1 with objects: 1(medium gray rubber cylinder) causes the blicket machine to go: off. Trial 2 with objects: 1(medium gray rubber cylinder), 2(medium green rubber cylinder) causes the blicket machine to go: on. Trial 3 with objects: 2(medium green rubber cylinder) causes the blicket machine to go: on. Trial 4 with objects: 3(medium gray rubber sphere), 4(medium yellow metal cube) causes the blicket machine to go: on. Trial 5 with objects: 5(medium blue metal sphere), 6(medium purple rubber cylinder), 3(medium gray rubber sphere) causes the blicket machine to go: off. Trial 6 with objects: 5(medium blue metal sphere), 6(medium purple rubber cylinder), 4(medium yellow metal cube), 7(medium yellow metal sphere) causes the blicket machine to go: on. Will the query with objects: 1(medium gray rubber cylinder), 5(medium blue metal sphere) activate the blicket? No.

Table 1. Example rationales generated by our LRR model on CATER.

Model	Compositional					Systematic				
	All	D.R.	I.D.	S.O.	B.B.	All	D.R.	I.D.	S.O.	B.B.
CNN-BERT (Ding et al., 2021)	43.7	54.0	46.8	40.5	28.7	39.9	55.9	68.2	0.0	45.5
NS-OPT (Zhang et al., 2021)	69.0	92.5	76.0	88.3	13.4	67.4	94.7	88.3	82.7	16.0
ALOE (Ding et al., 2021)	91.7	97.1	90.8	96.8	78.8	93.9	97.1	71.2	98.9	94.4
OPT-125M+CLIP	83.6	95.7	70.5	87.8	67.4	83.8	95.0	68.1	87.1	74.6
OPT-125M+ViT	96.9	99.4	95.0	97.3	93.5	96.7	99.1	95.0	98.3	93.3
LRR (w/o Surrogate Re-ID)	89.7	97.6	68.3	85.4	92.3	90.2	97.5	74.7	84.3	94.2
LRR (Ours)	99.3	99.8	98.5	99.5	98.7	99.0	99.8	98.4	99.8	97.6

Table 2. Evaluation on the ACRE dataset, where, D.R. – Direct evidence, I.D. – Indirect evidence, S.O. – Screened-off and B.B. – Backward Blocked subsets.

or enumerate objects present in the scene, to track or re-identify objects in the case of video, or to understand spatial relationships between multiple objects in the scene. Current state-of-the-art LLMs do not possess the ability to parse low-level visual information. A possible solution to circumvent the lack of low-level visual skills in LLMs is to combine them with low-level vision modules that can perform detection or tracking (Ding et al., 2021; Gupta & Kembhavi, 2022; Surfis et al., 2023). However, such an approach limits scalability across tasks due to the dependence on task-specific low-level vision modules. In this work, we instead explore an alternative solution, based on the generic vision features produced by a CNN like ResNet. This design choice yields a model that is trainable end-to-end and low-level visual skills can be instilled by fine-tuning it on appropriate *surrogate tasks* expressed in natural language.

In our LRR model, we leverage the flexibility of LLMs to express diverse low-level visual tasks through language in a generalized setup. Consider the visual reasoning problem from CLEVR in Figure 1, which requires low-level skills of object recognition and spatial reasoning. In this case, we design rationales with surrogate tasks as follows: For the low-level skill of object recognition, we introduce the surrogate task of explicitly listing all objects in the scene. Similarly, for spatial reasoning skills, we design rationales where we introduce the surrogate task of explicitly listing all objects left/right/front/behind a certain target object. This enables

the model to understand the spatial relation of the target object to other objects in the scene. Moreover, for visual reasoning problems that require tracking or re-identification, we introduce the surrogate task of predicting the positions or identifying the target objects across video frames in the rationale. Including low-level visual tasks in the rationale has the additional benefit that the solutions to these tasks remain within the context window of the LLM so that they are in fact “remembered” by the LLM and can be exploited to “reason” and solve subsequent tasks. The experiments section provides practical details on rationale construction.

4. Experiments

We now evaluate our model on visual reasoning tasks from: ACRE (Zhang et al., 2021) which focuses on the discovery of causal structures, CLEVR (Johnson et al., 2017) which focuses on spatial reasoning and CATER (Girdhar & Ramanan, 2020) which focus on temporal reasoning. We first evaluate dataset specific fine-tuned variants of our LRR model for fair comparison to prior work, followed by a variant jointly trained on ACRE, CLEVR and CATER.

Models and training details. We focus on the OPT family of LLMs (Zhang et al., 2022b), particularly OPT-125M and OPT-1.3B. We train our LRR model on a single Nvidia A100 GPU. We used a ResNet-101 (He et al., 2016) as the vision backbone across all tasks (see Appendix).

Method	FT vision	Overall	Count	Exist	Compare Numbers	Query Attribute	Compare Attribute
CNN+LSTM+RN (Malinowski et al., 2018)	✓	95.5	90.1	97.8	93.6	97.9	97.1
CNN+LSTM+FILM (Perez et al., 2018)	✓	97.6	94.3	99.3	93.4	99.3	99.3
HAN+RN (Santoro et al., 2017)	✓	98.8	97.2	99.6	96.9	99.6	99.6
OCCAM (Wang et al., 2021)	✓	99.4	98.1	99.8	99.0	99.9	99.9
NS-VQA (Yi et al., 2018)	✓	99.7	99.9	99.9	99.8	99.8	99.8
MDETR (Kamath et al., 2021)	✓	99.7	99.3	99.9	99.4	99.9	99.9
CNN+LSTM+SAN (Johnson et al., 2017)	✗	68.5	52.2	71.1	73.5	85.3	52.3
LRR (w/o Surrogate Spatial Reasoning)	✗	51.4	40.2	59.1	55.8	53.1	61.6
LRR (Ours)	✗	97.9	95.6	98.7	98.7	98.5	98.3

Table 3. Evaluation on the CLEVR dataset, comparing to state-of-the-art.

4.1. ACRE

The ACRE dataset (Zhang et al., 2021) focuses on evaluating the performance of vision systems on the problem of causal induction. Specifically, the dataset focuses on the problem of causal discovery using “blicket” detection experiments, originally administered to children. Such experiments involve a blicket detector which activates when a blicket object is put on it. The experiment involves a series of context trials, in which various (combinations of) objects are placed on the blicket detector, and subjects are shown whether the detector is activated. They are then asked which objects or (novel) combinations of objects would activate the machine. The examples in the ACRE dataset follow the same experimental design: each example contains 6 context trials and 4 questions on whether a certain combination of objects would activate the blicket machine.

Rationale construction. The key low-level visual challenge in the ACRE dataset is to identify objects in the context trials and to detect whether the blicket machine is activated. Therefore, we design the rationale with the surrogate tasks of object recognition and re-identification across the context trials. The rationale for each context trial describes the objects present and also assigns an unique integer ID to allow for re-identification. Additionally, the rationale also identifies state of the blicket machine (on/off). From Table 1: Trial 1 with objects: 1(medium gray rubber cylinder) causes blicket machine to go: off. Finally, the rationale re-identifies the objects in the query image, e.g., from Table 1: Will the query with objects: 1(medium gray rubber cylinder), 5(medium blue metal sphere) activate the blicket? This allows our LRR model to exploit the (“remembered”) previous steps in the rationale to infer which context trials involved the objects in the query as well as the state of the blicket machine in the relevant trials. The model can then aggregate the information in the rationale to reason and arrive at the final answer.

Baselines and evaluation. We base our LRR models on the OPT-125M and ResNet-101 backbones. We also compare to several baselines in Table 2. To highlight the importance

of our rationale generation process, we consider a baseline without the surrogate re-identification task: LRR (w/o Surrogate Re-ID). To highlight the importance of spatial grid based features along with top-down attention, we consider (with surrogate Re-ID), 1. A OPT-125M model with visual input at the first OPT (token embedding) layer using (global) CLIP (Dosovitskiy et al., 2021) embeddings, as in FORMAGE(Driess et al., 2023). 2. A OPT-125M model with visual input at the first OPT (token embedding) layer, as in PaLM-E (Driess et al., 2023). The visual input is patch-based, from ViT (Dosovitskiy et al., 2021).

We see that without the surrogate Re-ID task, our LRR model shows weak performance. This highlights the importance of “Look, Remember, Reason” paradigm where we explicitly solve the crucial Re-ID task and “remember” the results for each context trial. The importance of spatial grid features is illustrated by the weak performance of the OPT-125M+CLIP model, which is unable to effectively capture low-level visual cues due the pooling introduced by the CLIP model. Although the OPT-125M+ViT model uses spatial grid features, it’s performance is limited by the lack of top-down attention guided by the rich representations of the LLM. Furthermore, LRR model outperforms the state-of-the-art ALOE (Ding et al., 2021) model by a large margin on both the compositional (where the training and test sets contain different visual features) and systematic splits (different numbers of activated machines in the context trials) of the ACRE dataset. The gain in performance is especially significant in the backward blocked subset (B.B.) where the blicketness cannot be inferred from correlation alone due to the presence of confounding objects and the indirect subset (I.D.) where information needs to be integrated from multiple context trials. This performance advantage is due to the step-by-step reasoning enabled by our rationales which allows the model to aggregate visual information across multiple context trials.

4.2. CLEVR

The CLEVR dataset contains 700k examples consisting of a query image, a question, and a functional program.

Method	Static Camera			Moving Camera		
	Top-1(↑)	Top-5(↑)	L1(grid;↓)	Top-1(↑)	Top-5(↑)	L1(grid;↓)
R3D LSTM (Girdhar & Ramanan, 2020)	60.2	81.8	1.2	28.6	63.3	1.7
R3D + NL LSTM (Girdhar & Ramanan, 2020)	46.2	69.9	1.5	38.6	70.2	1.5
ALOE (Ding et al., 2021)	74.0	94.0	0.44	59.7	90.1	0.69
OPNet [†] (Shamsian et al., 2020)	74.8	-	0.54	-	-	-
Hopper [†] (Zhou et al., 2021)	73.2	93.8	0.85	-	-	-
TFC V3D Depthwise [†] (Zhang, 2022)	79.7	95.5	0.47	-	-	-
LRR (w/o Surrogate Tracking)	61.7	82.4	0.73	49.3	65.8	1.23
LRR (Ours)	85.1	96.2	0.23	75.1	91.9	0.48

Table 4. Evaluation on the CATER dataset ([†]results reported only for static camera).

The images consist of synthetically rendered 3D objects of various sizes, shapes, materials, and colors. The questions are designed to require multiple reasoning steps and are compositional in nature.

Rationale construction. The functional programs in CLVER consist of simpler sub-routines that follow a tree-like execution structure. These sub-routines decompose questions into simpler low-level object recognition and spatial reasoning tasks such as object counting and searching for objects based on spatial positions or materials, among others – operations necessary to solve the visual reasoning problem. We convert these sub-routines into rationales with surrogate tasks (details in Appendix C).

Baselines and evaluation. We begin with a comparison to state-of-the-art models in Table 3. Additionally, to highlight the importance of rationales with surrogate object recognition and spatial reasoning tasks, we consider a LRR (w/o Surrogate Spatial Reasoning) baseline.

From the results in Table 3, we see that non-LLM-based methods such as MDETR (Kamath et al., 2021) or NS-VQA (Yi et al., 2018), perform the best. However, such methods use a fine-tuned vision backbone (FT vision), based on DETR (Carion et al., 2020) or Mask-RCNN (He et al., 2017). The advantage of a fine-tuned vision backbone on CLEVR is mainly due to improved object detection performance in the presence of occlusions. However, the use of a fine-tuned vision backbones like DETR or Mask-RCNN makes it more challenging to apply the same model architecture across diverse visual reasoning tasks, *e.g.* the moving camera split of CATER (*c.f.* Table 5). Furthermore, DETR or Mask-RCNN type backbones require bounding box annotations, which are not always available. Even without a fine-tuned vision backbone, our LRR model outperforms FiLM (Perez et al., 2018) which employs a fine-tuned ResNet-101.

Finally, our LRR model without rationales LRR (w/o Surrogate Spatial Reasoning), performs significantly worse. This shows the importance of our surrogate object recognition and spatial reasoning tasks. We illustrate example rationales and further detailed ablations in the Appendix C.

4.3. CATER

The CATER (Compositional Actions and Temporal Reasoning) dataset is designed to test the ability to recognize compositions of object movements that require long-term temporal reasoning. Like CLEVR, the CATER dataset also consists exclusively of synthetically rendered 3D objects of various sizes, shapes, materials, and color. The synthetic nature of the CATER dataset ensures the lack of implicit biases over scene and object structure and thus the focus of the dataset is exclusively on the temporal structure of object movements. This makes the CATER dataset ideal to measure the temporal reasoning abilities of the current state-of-the-art LLMs. Similar to (Ding et al., 2021), we focus on the hardest task from the CATER dataset, *i.e.*, adversarial target tracking under occlusion and containment. This task amounts to predicting the position of a special object, referred to as "snitch", at the end of each video sequence. This is challenging as the position of the "snitch" can be occluded or (recursively) contained within other objects at the end of the sequence. This task is posed as a classification problem over a 6×6 grid. There are two splits of the dataset, static camera, and moving camera. The moving camera split is more challenging as the grid position of a certain object becomes much harder to discern from a single frame and long-term spatio-temporal correlations need to be captured.

Rationale construction. Building on the insights from the CLEVR dataset, we decompose the final grid classification problem into a sequence of simpler problems, using rationales with multi-target tracking as a surrogate low-level visual task. The rationale contains the grid positions of the snitch at every video frame. Following the paradigm of "Look, Remember, Reason" we include the surrogate task of tracking the medium and large cones in the scene, as these objects can occlude the snitch. With our rationale, the predicted intermediate grid positions of the objects of interest, *e.g.*, the snitch and cones, are "remembered" by the LLM and can be used to reason about the final position of the snitch in case of recursive containment by the cones.

Baselines and evaluation. To highlight the importance of our rationale generation process, we consider a baseline

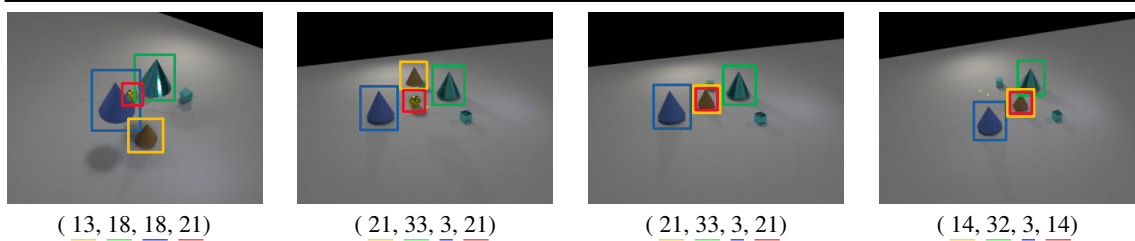


Table 5. Example rationales generated by our LRR model on CATER. The rationales contain the surrogate task of multi-target tracking. We show the predicted grid locations of the cones and the snitch below.

Method	Datasets						
	CLEVR	CATER: Static Camera		CATER: Moving Camera		ACRE: Comp	ACRE: Sys
	Acc \uparrow	Top 1 \uparrow	Top 5 \uparrow	Top 1 \uparrow	Top 5 \uparrow	Acc \uparrow	Acc \uparrow
LRR (Fine-tuned)	97.9	85.1	96.2	75.1	91.9	99.3	99.0
LRR (Joint)	97.3	83.7	96.5	75.2	92.8	98.9	98.7

Table 6. Evaluation of our LRR model trained jointly on CLEVR, CATER and ACRE (*c.f.* Tables 2 to 4).

where the rationale consists only of the grid positions of the snitch at every video frame, without the surrogate task of tracking the cones, LRR (w/o Surrogate Tracking). Both our LRR model and baselines are based on the OPT-125M backbone. Our LRR model is trained jointly on both the static and moving camera splits, similar to ALOE (Ding et al., 2021). The results are presented along with a comparison to state-of-the-art models in Table 4. Note that, OPNet (Shamsian et al., 2020), Hopper (Zhou et al., 2021), TFC V3D Depthwise (Zhang, 2022) and Loci (Traub et al., 2023) report results only on the static camera split. Loci (Traub et al., 2023) reports an impressive 90.7% accuracy on the static camera split, but it is not applicable to the moving camera split due to its static background and camera model.

Our LRR model outperforms TFC V3D Depthwise (Zhang, 2022) model on the static camera and ALOE (Ding et al., 2021) on the challenging moving camera split by a large margin. The large performance gain over the LRR (w/o Surrogate Tracking) baseline shows the advantage of using surrogate tracking tasks in the rationale. This shows that our rationales help capture long-term spatio-temporal correlations by “remembering” the intermediate positions of the objects of interest within the context window of the LLM. Without the multi-target tracking surrogate task, the model does not learn to track the cones and thus fails in cases of containment. We report qualitative examples in Table 5 and in Appendix D, which illustrates that our model is able to successfully track objects in cases of recursive containment and moving cameras.

4.4. Multi-dataset Training and Evaluation

Finally, we train our LRR model with OPT-1.3B and ResNet-101 backbones jointly on all three datasets: ACRE,

CLEVR and CATER in Table 6. Note that this is highly challenging due to the diverse nature of these tasks, which calls for different low and high level visual and reasoning skills. Despite these challenges, our jointly trained LRR model for the first time shows performance comparable to the dataset specific fine-tuned variants on such diverse visual reasoning tasks. This shows the ability of our LRR model to adapt to diverse visual reasoning tasks. A promising direction of future research would be joint training on an even larger set of visual reasoning datasets, potentially using larger LLM backbones and generalization to novel visual reasoning problems through in-context learning (Brown et al., 2020).

5. Conclusion

We show that off-the-shelf LLMs can solve complex visual reasoning tasks when supervised with rationales with surrogate visual tasks and equipped with top-down visual attention. We exploit the flexibility of LLMs in language modeling, which allows us to express diverse low-level visual tasks, *e.g.*, recognition, tracking, and re-identification, in the form of language. The use of off-the-shelf LLM and vision backbones allows our model to be readily applicable across diverse tasks. It outperforms the state-of-the-art by 7.6% and 5.1% on the compositional and systematic splits of the ACRE dataset and; by 5.4% Top-1 accuracy on static camera and 15.4% Top-1 accuracy on moving camera splits of the CATER dataset. Further, the performance of our LRR model is comparable to the state-of-the-art with task-specific architectures on CLEVR. While we obtain the best results through dataset specific fine-tuning, our LRR model jointly trained on ACRE, CLEVR and CATER performs favorably even through these datasets are highly diverse.

References

- Aghajanyan, A., Huang, B., Ross, C., Karpukhin, V., Xu, H., Goyal, N., Okhonko, D., Joshi, M., Ghosh, G., Lewis, M., and Zettlemoyer, L. CM3: A causal masked multimodal model of the internet. *CoRR*, abs/2201.07520, 2022.
- Alayrac, J., Donahue, J., Luc, P., Miech, A., Barr, I., Hasson, Y., Lenc, K., Mensch, A., Millican, K., Reynolds, M., Ring, R., Rutherford, E., Cabi, S., Han, T., Gong, Z., Samangooei, S., Monteiro, M., Menick, J. L., Borgeaud, S., Brock, A., Nematzadeh, A., Sharifzadeh, S., Binkowski, M., Barreira, R., Vinyals, O., Zisserman, A., and Simonyan, K. Flamingo: a visual language model for few-shot learning. In *NeurIPS*, 2022.
- Brown, T. B., Mann, B., Ryder, N., Subbiah, M., Kaplan, J., Dhariwal, P., Neelakantan, A., Shyam, P., Sastry, G., Askell, A., Agarwal, S., Herbert-Voss, A., Krueger, G., Henighan, T., Child, R., Ramesh, A., Ziegler, D. M., Wu, J., Winter, C., Hesse, C., Chen, M., Sigler, E., Litwin, M., Gray, S., Chess, B., Clark, J., Berner, C., McCandlish, S., Radford, A., Sutskever, I., and Amodei, D. Language models are few-shot learners. In *NeurIPS*, 2020.
- Carion, N., Massa, F., Synnaeve, G., Usunier, N., Kirillov, A., and Zagoruyko, S. End-to-end object detection with transformers. In *ECCV*, 2020.
- Chen, T., Saxena, S., Li, L., Lin, T., Fleet, D. J., and Hinton, G. E. A unified sequence interface for vision tasks. In *NeurIPS*, 2022.
- Chowdhery, A., Narang, S., Devlin, J., Bosma, M., Mishra, G., Roberts, A., Barham, P., Chung, H. W., Sutton, C., Gehrmann, S., Schuh, P., Shi, K., Tsvyashchenko, S., Maynez, J., Rao, A., Barnes, P., Tay, Y., Shazeer, N., Prabhakaran, V., Reif, E., Du, N., Hutchinson, B., Pope, R., Bradbury, J., Austin, J., Isard, M., Gur-Ari, G., Yin, P., Duke, T., Levskaya, A., Ghemawat, S., Dev, S., Michalewski, H., Garcia, X., Misra, V., Robinson, K., Fedus, L., Zhou, D., Ippolito, D., Luan, D., Lim, H., Zoph, B., Spiridonov, A., Sepassi, R., Dohan, D., Agrawal, S., Omernick, M., Dai, A. M., Pillai, T. S., Pellat, M., Lewkowycz, A., Moreira, E., Child, R., Polozov, O., Lee, K., Zhou, Z., Wang, X., Saeta, B., Diaz, M., Firat, O., Catasta, M., Wei, J., Meier-Hellstern, K., Eck, D., Dean, J., Petrov, S., and Fiedel, N. Palm: Scaling language modeling with pathways. *CoRR*, abs/2204.02311, 2022.
- Cobbe, K., Kosaraju, V., Bavarian, M., Hilton, J., Nakano, R., Hesse, C., and Schulman, J. Training verifiers to solve math word problems. *CoRR*, abs/2110.14168, 2021.
- d’Avila Garcez, A. S. and Lamb, L. C. Neurosymbolic AI: the 3rd wave. *CoRR*, abs/2012.05876, 2020.
- Ding, D., Hill, F., Santoro, A., Reynolds, M., and Botvinick, M. M. Attention over learned object embeddings enables complex visual reasoning. In *NeurIPS*, 2021.
- Dosovitskiy, A., Beyer, L., Kolesnikov, A., Weissenborn, D., Zhai, X., Unterthiner, T., Dehghani, M., Minderer, M., Heigold, G., Gelly, S., Uszkoreit, J., and Houlsby, N. An image is worth 16x16 words: Transformers for image recognition at scale. In *ICLR*, 2021.
- Dou, Z., Kamath, A., Gan, Z., Zhang, P., Wang, J., Li, L., Liu, Z., Liu, C., LeCun, Y., Peng, N., Gao, J., and Wang, L. Coarse-to-fine vision-language pre-training with fusion in the backbone. In *NeurIPS*, 2022.
- Driess, D., Xia, F., Sajjadi, M. S. M., Lynch, C., Chowdhery, A., Ichter, B., Wahid, A., Tompson, J., Vuong, Q., Yu, T., Huang, W., Chebotar, Y., Sermanet, P., Duckworth, D., Levine, S., Vanhoucke, V., Hausman, K., Toussaint, M., Greff, K., Zeng, A., Mordatch, I., and Florence, P. Palme: An embodied multimodal language model. *CoRR*, abs/2303.03378, 2023.
- Eichenberg, C., Black, S., Weinbach, S., Parcalabescu, L., and Frank, A. MAGMA - multimodal augmentation of generative models through adapter-based finetuning. In *EMNLP*, 2022.
- Gao, L., Biderman, S., Black, S., Golding, L., Hoppe, T., Foster, C., Phang, J., He, H., Thite, A., Nabeshima, N., Presser, S., and Leahy, C. The pile: An 800gb dataset of diverse text for language modeling. *CoRR*, abs/2101.00027, 2021.
- Girdhar, R. and Ramanan, D. CATER: A diagnostic dataset for compositional actions & temporal reasoning. In *ICLR*, 2020.
- Gupta, T. and Kembhavi, A. Visual programming: Compositional visual reasoning without training. *CoRR*, abs/2211.11559, 2022.
- He, K., Zhang, X., Ren, S., and Sun, J. Deep residual learning for image recognition. In *CVPR*, 2016.
- He, K., Gkioxari, G., Dollár, P., and Girshick, R. B. Mask R-CNN. In *ICCV*, 2017.
- Hu, R., Andreas, J., Rohrbach, M., Darrell, T., and Saenko, K. Learning to reason: End-to-end module networks for visual question answering. In *ICCV*, 2017.
- Hudson, D. A. and Manning, C. D. Compositional attention networks for machine reasoning. In *ICLR*, 2018.
- Ichter, B., Brohan, A., Chebotar, Y., Finn, C., Hausman, K., Herzog, A., Ho, D., Ibarz, J., Irpan, A., Jang, E., Julian, R., Kalashnikov, D., Levine, S., Lu, Y., Parada, C.,

- Rao, K., Sermanet, P., Toshev, A., Vanhoucke, V., Xia, F., Xiao, T., Xu, P., Yan, M., Brown, N., Ahn, M., Cortes, O., Sievers, N., Tan, C., Xu, S., Reyes, D., Rettinghouse, J., Quiambao, J., Pastor, P., Luu, L., Lee, K., Kuang, Y., Jesmonth, S., Joshi, N. J., Jeffrey, K., Ruano, R. J., Hsu, J., Gopalakrishnan, K., David, B., Zeng, A., and Fu, C. K. Do as I can, not as I say: Grounding language in robotic affordances. In *CoRL*, 2022.
- Jaegle, A., Gimeno, F., Brock, A., Vinyals, O., Zisserman, A., and Carreira, J. Perceiver: General perception with iterative attention. In *ICML*, 2021.
- Johnson, J., Hariharan, B., van der Maaten, L., Fei-Fei, L., Zitnick, C. L., and Girshick, R. B. CLEVR: A diagnostic dataset for compositional language and elementary visual reasoning. In *CVPR*, 2017.
- Kamath, A., Singh, M., LeCun, Y., Synnaeve, G., Misra, I., and Carion, N. MDETR - modulated detection for end-to-end multi-modal understanding. In *ICCV*, 2021.
- Kaplan, J., McCandlish, S., Henighan, T., Brown, T. B., Chess, B., Child, R., Gray, S., Radford, A., Wu, J., and Amodei, D. Scaling laws for neural language models. *CoRR*, abs/2001.08361, 2020.
- Koh, J. Y., Salakhutdinov, R., and Fried, D. Grounding language models to images for multimodal generation. *CoRR*, abs/2301.13823, 2023.
- Kojima, T., Gu, S. S., Reid, M., Matsuo, Y., and Iwasawa, Y. Large language models are zero-shot reasoners. In *NeurIPS*, 2022.
- Lewkowycz, A., Andreassen, A., Dohan, D., Dyer, E., Michalewski, H., Ramasesh, V. V., Slone, A., Anil, C., Schlag, I., Gutman-Solo, T., Wu, Y., Neysabur, B., Gur-Ari, G., and Misra, V. Solving quantitative reasoning problems with language models. In *NeurIPS*, 2022.
- Li, J., Li, D., Xiong, C., and Hoi, S. C. H. BLIP: bootstrapping language-image pre-training for unified vision-language understanding and generation. In *ICML*, 2022.
- Li, J., Li, D., Savarese, S., and Hoi, S. C. H. BLIP-2: bootstrapping language-image pre-training with frozen image encoders and large language models. *CoRR*, abs/2301.12597, 2023.
- Li, Z., Stengel-Eskin, E., Zhang, Y., Xie, C., Tran, Q., Durme, B. V., and Yuille, A. L. Calibrating concepts and operations: Towards symbolic reasoning on real images. In *ICCV*, 2021.
- Ling, W., Yogatama, D., Dyer, C., and Blunsom, P. Program induction by rationale generation: Learning to solve and explain algebraic word problems. In *ACL*, 2017.
- Liu, H., Li, C., Wu, Q., and Lee, Y. J. Visual instruction tuning. *CoRR*, abs/2304.08485, 2023.
- Loshchilov, I. and Hutter, F. Decoupled weight decay regularization. In *ICLR*, 2019.
- Lu, P., Peng, B., Cheng, H., Galley, M., Chang, K., Wu, Y. N., Zhu, S., and Gao, J. Chameleon: Plug-and-play compositional reasoning with large language models. *CoRR*, abs/2304.09842, 2023.
- Mahajan, S. and Roth, S. Diverse image captioning with context-object split latent spaces. In *NeurIPS*, 2020.
- Malinowski, M., Doersch, C., Santoro, A., and Battaglia, P. W. Learning visual question answering by bootstrapping hard attention. In *ECCV*, 2018.
- Mañas, O., López, P. R., Ahmadi, S., Nematzadeh, A., Goyal, Y., and Agrawal, A. MAPL: parameter-efficient adaptation of unimodal pre-trained models for vision-language few-shot prompting. In *EACL*, 2023.
- Marcus, G. Deep learning: A critical appraisal. *CoRR*, abs/1801.00631, 2018.
- Marcus, G. The next decade in AI: four steps towards robust artificial intelligence. *CoRR*, abs/2002.06177, 2020.
- Mondal, S. S., Webb, T., and Cohen, J. D. Learning to reason over visual objects. *CoRR*, abs/2303.02260, 2023.
- Nye, M. I., Andreassen, A. J., Gur-Ari, G., Michalewski, H., Austin, J., Bieber, D., Dohan, D., Lewkowycz, A., Bosma, M., Luan, D., Sutton, C., and Odena, A. Show your work: Scratchpads for intermediate computation with language models. *CoRR*, abs/2112.00114, 2021.
- OpenAI. GPT-4 technical report. *CoRR*, abs/2303.08774, 2023.
- Perez, E., Strub, F., de Vries, H., Dumoulin, V., and Courville, A. C. Film: Visual reasoning with a general conditioning layer. In *AAAI*, 2018.
- Radford, A., Kim, J. W., Hallacy, C., Ramesh, A., Goh, G., Agarwal, S., Sastry, G., Askell, A., Mishkin, P., Clark, J., Krueger, G., and Sutskever, I. Learning transferable visual models from natural language supervision. In *ICML*, 2021.
- Rae, J. W., Borgeaud, S., Cai, T., Millican, K., Hoffmann, J., Song, H. F., Aslanides, J., Henderson, S., Ring, R., Young, S., Rutherford, E., Hennigan, T., Menick, J., Cassirer, A., Powell, R., van den Driessche, G., Hendricks, L. A., Rauh, M., Huang, P., Glaese, A., Welbl, J., Dhathathri, S., Huang, S., Uesato, J., Mellor, J., Higgins, I., Creswell, A., McAleese, N., Wu, A., Elsen, E., Jayakumar, S. M., Buchatskaya, E., Budden, D., Sutherland, E., Simonyan,

- K., Paganini, M., Sifre, L., Martens, L., Li, X. L., Kuncoro, A., Nematzadeh, A., Gribovskaya, E., Donato, D., Lazaridou, A., Mensch, A., Lespiau, J., Tsimpoukelli, M., Grigorev, N., Fritz, D., Sottiaux, T., Pajarskas, M., Pohlen, T., Gong, Z., Toyama, D., de Masson d'Autume, C., Li, Y., Terzi, T., Mikulik, V., Babuschkin, I., Clark, A., de Las Casas, D., Guy, A., Jones, C., Bradbury, J., Johnson, M. J., Hechtman, B. A., Weidinger, L., Gabriel, I., Isaac, W., Lockhart, E., Osindero, S., Rimell, L., Dyer, C., Vinyals, O., Ayoub, K., Stanway, J., Bennett, L., Hassabis, D., Kavukcuoglu, K., and Irving, G. Scaling language models: Methods, analysis & insights from training gopher. *CoRR*, abs/2112.11446, 2021.
- Raffel, C., Shazeer, N., Roberts, A., Lee, K., Narang, S., Matena, M., Zhou, Y., Li, W., and Liu, P. J. Exploring the limits of transfer learning with a unified text-to-text transformer. *CoRR*, abs/1910.10683, 2019.
- Rahaman, N., Gondal, M. W., Joshi, S., Gehler, P. V., Bengio, Y., Locatello, F., and Schölkopf, B. Dynamic inference with neural interpreters. In *NeurIPS*, 2021.
- Rahman, T., Lee, H., Ren, J., Tulyakov, S., Mahajan, S., and Sigal, L. Make-a-story: Visual memory conditioned consistent story generation. In *CVPR*, 2023.
- Rajani, N. F., McCann, B., Xiong, C., and Socher, R. Explain yourself! leveraging language models for common-sense reasoning. In *ACL*, 2019.
- Recchia, G. Teaching autoregressive language models complex tasks by demonstration. *CoRR*, abs/2109.02102, 2021.
- Sajjadi, M. S. M., Duckworth, D., Mahendran, A., van Steenkiste, S., Pavetic, F., Lucic, M., Guibas, L. J., Greff, K., and Kipf, T. Object scene representation transformer. In *NeurIPS*, 2022.
- Salewski, L., Koepke, A. S., Lensch, H. P. A., and Akata, Z. Clevr-x: A visual reasoning dataset for natural language explanations. In *xxAI - Beyond explainable Artificial Intelligence*. Springer, 2022.
- Sanh, V., Webson, A., Raffel, C., Bach, S. H., Sutawika, L., Alyafeai, Z., Chaffin, A., Stiegler, A., Raja, A., Dey, M., Bari, M. S., Xu, C., Thakker, U., Sharma, S. S., Szczechla, E., Kim, T., Chhablani, G., Nayak, N. V., Datta, D., Chang, J., Jiang, M. T., Wang, H., Manica, M., Shen, S., Yong, Z. X., Pandey, H., Bawden, R., Wang, T., Neeraj, T., Rozen, J., Sharma, A., Santilli, A., Févry, T., Fries, J. A., Teehan, R., Scao, T. L., Biderman, S., Gao, L., Wolf, T., and Rush, A. M. Multitask prompted training enables zero-shot task generalization. In *ICLR*, 2022.
- Santoro, A., Raposo, D., Barrett, D. G. T., Malinowski, M., Pascanu, R., Battaglia, P. W., and Lillicrap, T. A simple neural network module for relational reasoning. In *NeurIPS*, 2017.
- Scao, T. L., Fan, A., Akiki, C., Pavlick, E., Ilic, S., Hesslow, D., Castagné, R., Luccioni, A. S., Yvon, F., Gallé, M., Tow, J., Rush, A. M., Biderman, S., Webson, A., Ammanamanchi, P. S., Wang, T., Sagot, B., Muennighoff, N., del Moral, A. V., Ruwase, O., Bawden, R., Bekman, S., McMillan-Major, A., Beltagy, I., Nguyen, H., Saulnier, L., Tan, S., Suarez, P. O., Sanh, V., Laurençon, H., Jernite, Y., Launay, J., Mitchell, M., Raffel, C., Gokaslan, A., Simhi, A., Soroa, A., Aji, A. F., Alfassy, A., Rogers, A., Nitzav, A. K., Xu, C., Mou, C., Emezue, C., Klamm, C., Leong, C., van Strien, D., Adelani, D. I., and et al. BLOOM: A 176b-parameter open-access multilingual language model. *CoRR*, abs/2211.05100, 2022.
- Shamsian, A., Kleinfeld, O., Globerson, A., and Chechik, G. Learning object permanence from video. In *ECCV*, 2020.
- Strub, F., Seurin, M., Perez, E., de Vries, H., Mary, J., Preux, P., Courville, A. C., and Pietquin, O. Visual reasoning with multi-hop feature modulation. In *ECCV*, 2018.
- Surís, D., Menon, S., and Vondrick, C. Vipergpt: Visual inference via python execution for reasoning. *CoRR*, abs/2303.08128, 2023.
- Touvron, H., Lavril, T., Izacard, G., Martinet, X., Lachaux, M., Lacroix, T., Rozière, B., Goyal, N., Hambro, E., Azhar, F., Rodriguez, A., Joulin, A., Grave, E., and Lample, G. Llama: Open and efficient foundation language models. *CoRR*, abs/2302.13971, 2023.
- Traub, M., Otte, S., Menge, T., Karlbauer, M., Thümmel, J., and Butz, M. V. Learning what and where - unsupervised disentangling location and identity tracking. In *ICLR*, 2023.
- Tsimpoukelli, M., Menick, J., Cabi, S., Eslami, S. M. A., Vinyals, O., and Hill, F. Multimodal few-shot learning with frozen language models. In *NeurIPS*, 2021.
- Vaswani, A., Shazeer, N., Parmar, N., Uszkoreit, J., Jones, L., Gomez, A. N., Kaiser, L., and Polosukhin, I. Attention is all you need. In *NeurIPS*, 2017.
- Wang, X., Wei, J., Schuurmans, D., Le, Q. V., Chi, E. H., and Zhou, D. Self-consistency improves chain of thought reasoning in language models. *CoRR*, abs/2203.11171, 2022.
- Wang, Z., Wang, K., Yu, M., Xiong, J., Hwu, W., Hasegawa-Johnson, M., and Shi, H. Interpretable visual reasoning via induced symbolic space. In *ICCV*, 2021.

- Wei, J., Bosma, M., Zhao, V. Y., Guu, K., Yu, A. W., Lester, B., Du, N., Dai, A. M., and Le, Q. V. Finetuned language models are zero-shot learners. *CoRR*, abs/2109.01652, 2021.
- Wei, J., Wang, X., Schuurmans, D., Bosma, M., brian ichter, Xia, F., Chi, E. H., Le, Q. V., and Zhou, D. Chain of thought prompting elicits reasoning in large language models. In *NeurIPS*, 2022a.
- Wei, J., Wang, X., Schuurmans, D., Bosma, M., Ichter, B., Xia, F., Chi, E. H., Le, Q. V., and Zhou, D. Chain-of-thought prompting elicits reasoning in large language models. In *NeurIPS*, 2022b.
- Yao, S., Zhao, J., Yu, D., Du, N., Shafran, I., Narasimhan, K., and Cao, Y. React: Synergizing reasoning and acting in language models. *CoRR*, abs/2210.03629, 2022.
- Yao, Y., Xu, J., Wang, F., and Xu, B. Cascaded mutual modulation for visual reasoning. In *EMNLP*, 2018.
- Ye, Q., Xu, H., Xu, G., Ye, J., Yan, M., Zhou, Y., Wang, J., Hu, A., Shi, P., Shi, Y., Li, C., Xu, Y., Chen, H., Tian, J., Qi, Q., Zhang, J., and Huang, F. mplug-owl: Modularization empowers large language models with multimodality. *CoRR*, abs/2304.14178, 2023.
- Yi, K., Wu, J., Gan, C., Torralba, A., Kohli, P., and Tenenbaum, J. Neural-symbolic VQA: disentangling reasoning from vision and language understanding. In *NeurIPS*, 2018.
- Zhang, C., Jia, B., Edmonds, M., Zhu, S., and Zhu, Y. ACRE: abstract causal reasoning beyond covariation. In *CVPR*, 2021.
- Zhang, C., Xie, S., Jia, B., Wu, Y. N., Zhu, S., and Zhu, Y. Learning algebraic representation for systematic generalization in abstract reasoning. In *ECCV*, 2022a.
- Zhang, R., Han, J., Zhou, A., Hu, X., Yan, S., Lu, P., Li, H., Gao, P., and Qiao, Y. Llama-adapter: Efficient fine-tuning of language models with zero-init attention. *CoRR*, abs/2303.16199, 2023a.
- Zhang, S. Tfcnet: Temporal fully connected networks for static unbiased temporal reasoning. *CoRR*, 2022.
- Zhang, S., Roller, S., Goyal, N., Artetxe, M., Chen, M., Chen, S., Dewan, C., Diab, M. T., Li, X., Lin, X. V., Mihaylov, T., Ott, M., Shleifer, S., Shuster, K., Simig, D., Koura, P. S., Sridhar, A., Wang, T., and Zettlemoyer, L. OPT: open pre-trained transformer language models. *CoRR*, abs/2205.01068, 2022b.
- Zhang, Z., Zhang, A., Li, M., Zhao, H., Karypis, G., and Smola, A. Multimodal chain-of-thought reasoning in language models. *CoRR*, abs/2302.00923, 2023b.
- Zhou, H., Kadav, A., Lai, F., Niculescu-Mizil, A., Min, M. R., Kapadia, M., and Graf, H. P. Hopper: Multi-hop transformer for spatiotemporal reasoning. In *ICLR*, 2021.

A. Overview of Appendices

Here we provide, 1. Additional training details including hyper-parameters used for evaluation in Section 4 of the main paper across CLEVR, CATER and ACRE datasets. 2. Additional details of the rationale construction process for the CLEVR dataset (*c.f.* Section 4.1 *Rationale construction* in the main paper). 3. Additional experiments to highlight the importance of rationales on the CLEVR dataset. 4. Additional ablations on the structure of rationales used in the CLEVR dataset. 5. Additional qualitative examples across CLEVR, CATER and ACRE datasets.

B. ACRE

Additional training details. We trained our LRR model with the OPT-125M backbone until convergence ($\sim 500k$ iterations) with a batch size of 1. We use the AdamW optimizer (Loshchilov & Hutter, 2019) with a learning rate of 1×10^{-5} , $\beta_1 = 0.9$, $\beta_2 = 0.95$ and λ (weight decay) = 0.1 and gradient clipping with a norm of 1.0.

Additional qualitative examples. We include additional qualitative examples in Table 7, along with our rationales. These examples illustrate that using our surrogate re-identification task, our LRR model can aggregate information from multiple context trials to arrive at the final answer – following the paradigm of “Look, Remember, Reason”.

C. CLEVR

Additional training details. We trained our LRR model with the OPT-1.3B backbone for 2 epochs (inline with prior work (Santoro et al., 2017)) with a batch size of 1. We use the AdamW optimizer (Loshchilov & Hutter, 2019) with a learning rate of 1×10^{-5} , $\beta_1 = 0.9$, $\beta_2 = 0.95$ and λ (weight decay) = 0.1. We use gradient clipping with a norm of 1.0.

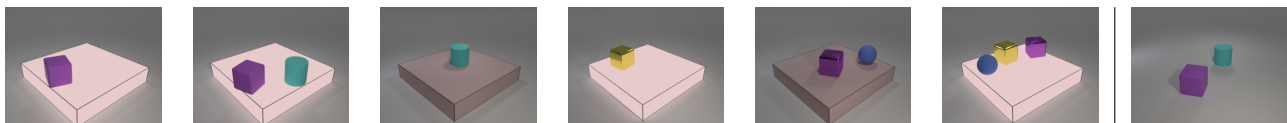
Rationale construction. As discussed in the main paper, we use the functional programs in the CLEVR dataset to construct rationales. The functional programs consist of simpler sub-routines that follow a tree-like execution structure. The sub-routines are converted into sentences using templates shown in Table 8. These templates are designed to include surrogate tasks, *e.g.*, object recognition or object localization, important for spatial reasoning in CLEVR. In detail, for the “Scene” sub-routine, the rationale requires the model to explicitly list (thus recognize) all objects in the scene including their size, color, material and shape. For the “Relate” sub-routine the rationale requires the model to explicitly list all objects at the front, behind, left or right of a target object with their spatial positions in the scene. Once these surrogate tasks have been solved, the solution remains within the context window of the model and is thus “remembered” by the model for subsequent tasks.

Additional qualitative examples. We include additional qualitative examples including rationales with surrogate tasks in Table 11.

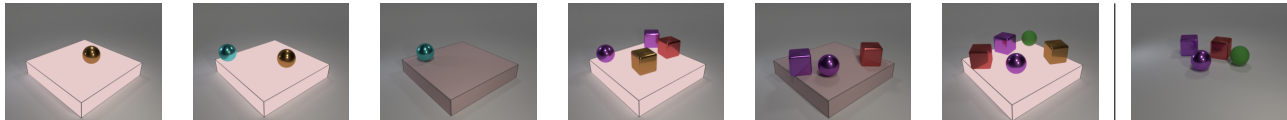
Importance of rationales. We highlight the importance of rationales with surrogate tasks for visual reasoning on the CLEVR dataset in Table 9. To this end, here we further investigate the performance of our LRR (w/o Surrogate Spatial Reasoning) baseline, which shows weak performance in Table 3. We evaluate this baseline with various OPT model sizes: 125M, 1.3B and 6.7B. Additionally, we consider an *Oracle-Perception* baseline, that does not generate rationales but receives a ground truth list of objects and their corresponding positions as a prompt in addition to the query image. This baseline essentially has near perfect vision, *i.e.*, it receives all visual information essential for answering the question in the prompt. However, it lacks step-by-step reasoning capabilities.

We observe in Table 9 that without our low-level surrogate tasks, accuracy does not improve substantially even with larger LLM model sizes. Further, we observe that while the Oracle-Perception baseline is provided all necessary visual information to the model via the prompt, it is unable to use this information effectively without the step-by-step reasoning process enabled by our rationales. Thus, rationales with our low-level surrogate tasks are crucial for visual reasoning on the CLEVR dataset.

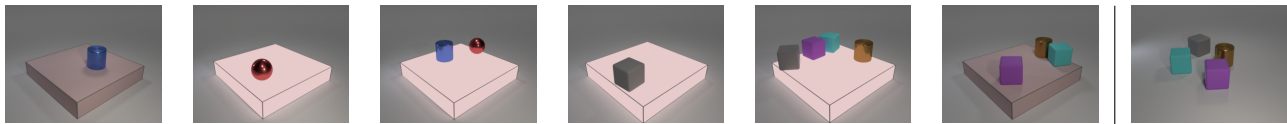
Rationale types. Here, we evaluate the effectiveness of our proposed rationales that enables our LRR model to “Look, Remember, Reason”. To do this, we consider alternative rationale types. First, we consider the *Object-List-Position* rationale that generates the list of objects and their corresponding positions in the scene. This enables the model to extract relevant visual features from the query image but does not enable step-by-step reasoning. Secondly, we consider rationales from the CLEVR-X dataset (Salewski et al., 2022). These rationales describe the reasoning and visual information that is necessary



Rationale: The task is to detect whether the following combination of objects activate the blicket machine, which activates when we put a blicket on it. Next, we will conduct six trials where we put a combination of objects on the machine. Trial 1 with objects: 1(medium purple rubber cube) causes the blicket machine to go: on. Trial 2 with objects: 1(medium purple rubber cube), 2(medium cyan rubber cylinder) causes the blicket machine to go: on. Trial 3 with objects: 2(medium cyan rubber cylinder) causes the blicket machine to go: off. Trial 4 with objects: 3(medium yellow metal cube) causes the blicket machine to go: on. Trial 5 with objects: 4(medium purple metal cube), 5(medium blue rubber sphere) causes the blicket machine to go: off. Trial 6 with objects: 5(medium blue rubber sphere), 3(medium yellow metal cube), 4(medium purple metal cube) causes the blicket machine to go: on. Will the query with objects: 1(medium purple rubber cube), 2(medium cyan rubber cylinder) activate the blicket? Yes.



Rationale: The task is to detect whether the following combination of objects activate the blicket machine, which activates when we put a blicket on it. Next, we will conduct six trials where we put a combination of objects on the machine. Trial 1 with objects: 1(medium brown metal sphere) causes the blicket machine to go: on. Trial 2 with objects: 2(medium cyan metal sphere), 1(medium brown metal sphere) causes the blicket machine to go: on. Trial 3 with objects: 2(medium cyan metal sphere) causes the blicket machine to go: off. Trial 4 with objects: 3(medium purple metal sphere), 4(medium brown metal cube), 5(medium purple metal cube), 6(medium red metal cube) causes the blicket machine to go: on. Trial 5 with objects: 5(medium purple metal cube), 3(medium purple metal sphere), 6(medium red metal cube) causes the blicket machine to go: off. Trial 6 with objects: 6(medium red metal cube), 5(medium purple metal cube), 3(medium purple metal sphere), 7(medium green rubber sphere), 4(medium brown metal cube) causes the blicket machine to go: on. Will the query with objects: 5(medium purple metal cube), 3(medium purple metal sphere), 6(medium red metal cube), 7(medium green rubber sphere) activate the blicket? Maybe.



Rationale: The task is to detect whether the following combination of objects activate the blicket machine, which activates when we put a blicket on it. Next, we will conduct six trials where we put a combination of objects on the machine. Trial 1 with objects: 1(medium blue metal cylinder) causes the blicket machine to go: off. Trial 2 with objects: 2(medium red metal sphere) causes the blicket machine to go: on. Trial 3 with objects: 1(medium blue metal cylinder), 2(medium red metal sphere) causes the blicket machine to go: on. Trial 4 with objects: 3(medium gray rubber cube) causes the blicket machine to go: on. Trial 5 with objects: 3(medium gray rubber cube), 4(medium purple rubber cube), 5(medium cyan rubber cube), 6(medium brown metal cylinder) causes the blicket machine to go: on. Trial 6 with objects: 4(medium purple rubber cube), 6(medium brown metal cylinder), 5(medium cyan rubber cube) causes the blicket machine to go: off. Will the query with objects: 5(medium cyan rubber cube), 3(medium gray rubber cube), 4(medium purple rubber cube), 6(medium brown metal cylinder) activate the blicket? Yes.

Table 7. Example rationales generated by our LRR model on CATER.

to answer a given question. However, they are concise and do not enable step-by-step reasoning. We report the results in Table 10. Finally, we consider a variant of our “Look, Remember, Reason” rationales that does not include the surrogate task of inferring spatial relations (w/o Spatial Relations), corresponding to the sub-routine “Relate” as detailed in Table 10.

The performance of our LRR model with Object-List-Position and CLEVR-X(Salewski et al., 2022) rationales is significantly worse (c.f. Table 1 in the main paper). This is because the Object-List-Position rationales do not allow for step-by-step reasoning and the CLEVR-X rationales are too concise – thus not all important steps required to arrive at the final answer are included in the rationale. Finally, we see that removing surrogate tasks from the rationale as in the LRR (w/o Surrogate Spatial Relations) baseline has an adverse effect on performance. This again highlights the importance of surrogate tasks.

D. CATER

Additional training details. We trained our LRR model with the OPT-125M backbone until convergence (~ 600k iterations) with a batch size of 1. We use the AdamW optimizer (Loshchilov & Hutter, 2019) with a learning rate of

Look, Remember and Reason: Visual Reasoning with Grounded Rationales

Sub-routine	Input	Rationale Template
Scene	objects	Step i , the objects in the scene are <[size,color,material,shape] objects>.
Filter	objects, attribute, value	Step j , from i , the objects of <attribute, value> are <[size,color,material,shape] objects>.
Relate	<i>front</i> , object	Step j , from i , the objects in the scene in front of <object> are <[size,color,material,shape] object> at <pos>, ..., <[size,color,material,shape] object> at <pos>.
Relate	<i>behind</i> , object	Step j , from i , the objects in the scene behind <object> are <[size,color,material,shape] object> at <pos>, ..., <[size,color,material,shape] object> at <pos>.
Relate	<i>left</i> , object	Step j , from i , the objects in the scene at the left of <object> are <[size,color,material,shape] object> at <pos>, ..., <[size,color,material,shape] object> at <pos>.
Relate	<i>right</i> , object	Step j , from i , the objects in the scene at the right of <object> are <[size,color,material,shape] object> at <pos>, ..., <[size,color,material,shape] object> at <pos>.
Intersect	objects	Step k , from i and j , the common objects are <[size,color,material,shape] object in objects>.
Union	objects	Step k , from i and j , the common objects are <[size,color,material,shape] object in objects>.
Query	<i>attribute</i> , value, object	Step j , from i , the <attribute> of the <[size,color,material,shape] object> is <value>.
Equal	objects	Step k , from i and j , there are an equal number of objects.
Less, More	objects	Step k , from i and j , there are less/more objects in step i than j .
Exist	object	Step j , from i , there is such an object / there is no such object.
Count	objects	Step j , from i , there are <number of objects> such objects.
Equal	<i>attribute</i> , objects	Step j , from i , the objects <[size,color,material,shape] object> and <[size,color,material,shape] object> have/ do not have the same <attribute>.
Unique	objects	Step j , from i , the object is unique.

Table 8. Example rationale templates for sub-routines in CLEVR (*c.f.* Figure 2 in Johnson et al. (2017)).

Method	OPT Model Size	Accuracy
LRR (w/o Surrogate Spatial Reasoning)	125M	50.9
LRR (w/o Surrogate Spatial Reasoning)	1.3B	51.4
LRR (w/o Surrogate Spatial Reasoning)	6.7B	53.4
Oracle-Perception	1.3B	51.5

Table 9. Evaluation of LRR baselines without rationales.

1×10^{-5} , $\beta_1 = 0.9$, $\beta_2 = 0.95$ and λ (weight decay) = 0.1. We use gradient clipping with a norm of 1.0.

As discussed in the main paper, we train a joint model for the static and moving camera splits. In order to deal with the limited training set size, we augment the training set by *jittering* the grid positions of the cones and the snitch. In detail, jittering grid positions means that we replace the groundtruth grid position with a neighbouring (8 connected) grid position with a fixed probability (we found 0.25 to be adequate). Note that, only the input sequence to the LLM is jittered and the target sequence remains unperturbed.

Additional qualitative examples. We include additional qualitative examples including both the static and moving camera splits in Table 12. We see that our LRR model can successfully deal with containment in both static camera (rows 1-3; Table 12) and moving camera (row 4-5; Table 12) settings, due to our rationale that explicitly tracks cones and the snitch. Note that the example in row 5 in Table 12 from the moving camera split is especially challenging due to recursive containment.

Method	Accuracy
LRR (Object-List-Position)	69.2
LRR (CLEVR-X Salewski et al. (2022))	72.2
LRR (w/o Spatial Relations)	94.2

Table 10. Evaluation of rationale types (OPT-1.3B).

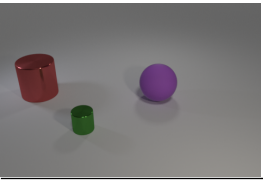
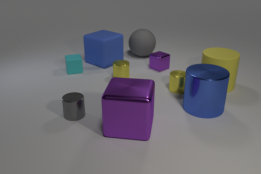
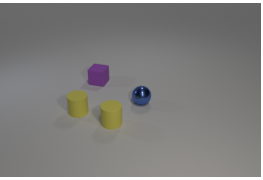
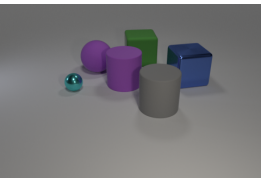
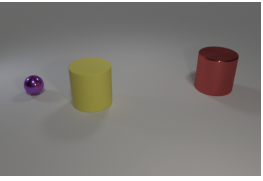
Query Image	Rationale
	<p>Question: What number of things are shiny cylinders that are in front of the large rubber thing or purple matte things?</p> <p>Rationale: Step 1, the objects in the scene are large red metal cylinder, small green metal cylinder, large purple rubber sphere. Step 2, from step 1, the objects of size large, material rubber are large purple rubber sphere. Step 3, from step 2, this object is unique. Step 4, in front of the large purple rubber sphere at (58,29) the objects in the scene are small green metal cylinder at (30,43). Step 5, from step 4, the objects of material metal, shape cylinder are small green metal cylinder. Step 6, the objects in the scene are large red metal cylinder, small green metal cylinder, large purple rubber sphere. Step 7, from step 6, the objects of color purple, material rubber are large purple rubber sphere. Step 8, from steps 5 and 7, the common objects are small green metal cylinder, large purple rubber sphere. Step 9, from step 8, there are 2 such objects. The answer is, 2.</p>
	<p>Question: How many objects are cyan cylinders or tiny things to the left of the big rubber ball?</p> <p>Rationale: Step 1, the objects in the scene are small cyan rubber cube, small gray metal cylinder, large blue rubber cube, small yellow metal cylinder, large purple metal cube, large gray rubber sphere, small purple metal cube, small yellow metal cylinder, large blue metal cylinder, large yellow rubber cylinder. Step 2, from step 1, there are no objects of color cyan, shape cylinder. Step 3, the objects in the scene are small cyan rubber cube, small gray metal cylinder, large blue rubber cube, small yellow metal cylinder, large purple metal cube, large gray rubber sphere, small purple metal cube, small yellow metal cylinder, large blue metal cylinder, large yellow rubber cylinder. Step 4, from step 3, the objects of size large, material rubber, shape sphere are large gray rubber sphere. Step 5, from step 4, this object is unique. Step 6, at the left of the large gray rubber sphere at (52,15) the objects in the scene are small cyan rubber cube at (27,23), small gray metal cylinder at (27,39), large blue rubber cube at (38,17), small yellow metal cylinder at (44,25), large purple metal cube at (47,39). Step 7, from step 6, the objects of size small are small cyan rubber cube, small gray metal cylinder, small yellow metal cylinder. Step 8, from steps 2 and 7, the common objects are small cyan rubber cube, small gray metal cylinder, small yellow metal cylinder. Step 9, from step 8, there are 3 such objects. The answer is, 3.</p>
	<p>Question: How many objects are either big red spheres or small yellow cylinders in front of the purple rubber block?</p> <p>Rationale: Step 1, the objects in the scene are small yellow rubber cylinder, small purple rubber cube, small yellow rubber cylinder, small blue metal sphere. Step 2, from step 1, there are no objects of size large, color red, shape sphere. Step 3, the objects in the scene are small yellow rubber cylinder, small purple rubber cube, small yellow rubber cylinder, small blue metal sphere. Step 4, from step 3, the objects of color purple, material rubber, shape cube are small purple rubber cube. Step 5, from step 4, this object is unique. Step 6, in front of the small purple rubber cube at (36,26) the objects in the scene are small yellow rubber cylinder at (28,37), small yellow rubber cylinder at (41,41), small blue metal sphere at (52,34). Step 7, from step 6, the objects of size small, color yellow, shape cylinder are small yellow rubber cylinder, small yellow rubber cylinder. Step 8, from steps 2 and 7, the common objects are small yellow rubber cylinder, small yellow rubber cylinder. Step 9, from step 8, there are 2 such objects. The answer is, 2.</p>
	<p>Question: Is the material of the cylinder that is behind the tiny shiny ball the same as the object that is on the right side of the big gray matte thing?</p> <p>Rationale: Step 1, the objects in the scene are small cyan metal sphere, large purple rubber sphere, large purple rubber cylinder, large green rubber cube, large gray rubber cylinder, large blue metal cube. Step 2, from step 1, the objects of size small, material metal, shape sphere are small cyan metal sphere. Step 3, from step 2, this object is unique. Step 4, behind the small cyan metal sphere at (27,28) The objects in the scene are large purple rubber sphere at (35,19), large purple rubber cylinder at (45,23), large green rubber cube at (51,16), large blue metal cube at (69,22). Step 5, from step 4, the objects of shape cylinder are large purple rubber cylinder. Step 6, from step 5, this object is unique. Step 7, from step 6, the material of the large purple rubber cylinder is rubber. Step 8, the objects in the scene are small cyan metal sphere, large purple rubber sphere, large purple rubber cylinder, large green rubber cube, large gray rubber cylinder, large blue metal cube. Step 9, from step 8, the objects of size large, color gray, material rubber are large gray rubber cylinder. Step 10, from step 9, this object is unique. Step 11, at the right of the large gray rubber cylinder at (58,31) the objects in the scene are large blue metal cube at (69,22). Step 12, from step 11, this object is unique. Step 13, from step 12, the material of the large blue metal cube is metal. Step 14, from steps 7 and 13, the objects large purple rubber cylinder and large blue metal cube do not have the same material. The answer is, no.</p>
	<p>Question: What number of big rubber things are in front of the big object that is in front of the sphere?</p> <p>Rationale: Step 1, the objects in the scene are small purple metal sphere, large yellow rubber cylinder, large red metal cylinder. Step 2, from step 1, the objects of shape sphere are small purple metal sphere. Step 3, from step 2, this object is unique. Step 4, in front of the small purple metal sphere at (12,30) the objects in the scene are large yellow rubber cylinder. Step 5, from step 4, the objects of size large are large yellow rubber cylinder. Step 6, from step 5, this object is unique. Step 7, in front of the large yellow rubber cylinder at (33,30) there are no objects in the scene. Step 8, from step 7, there are no objects of size large, material rubber. Step 9, from step 8, there are 0 such objects. The answer is, 0</p>

Table 11. Example rationales generated by our LRR model on CLEVR.

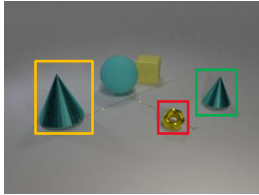
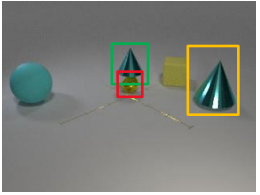
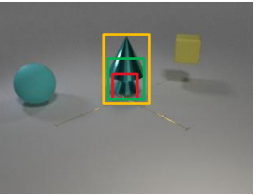
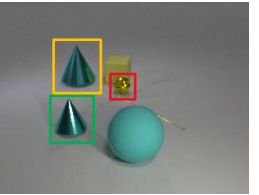
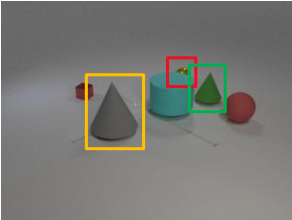
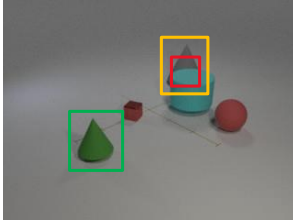
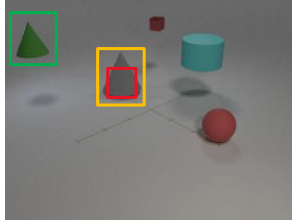
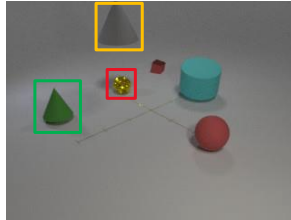
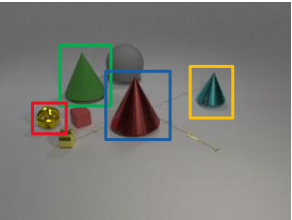
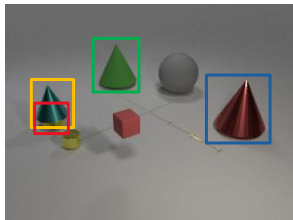
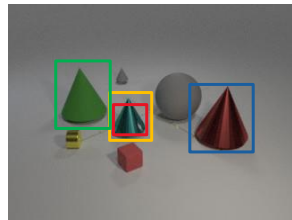
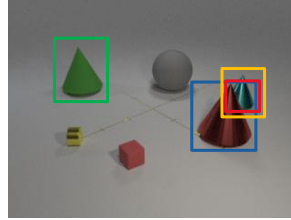
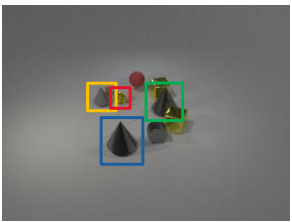
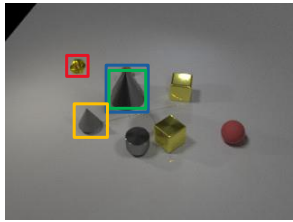
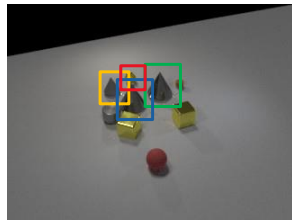
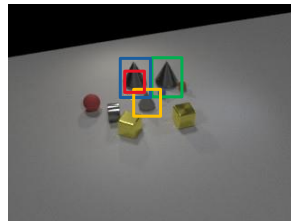
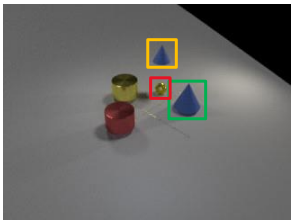
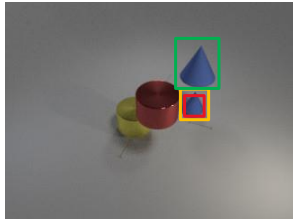
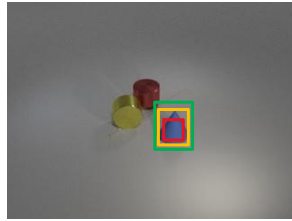
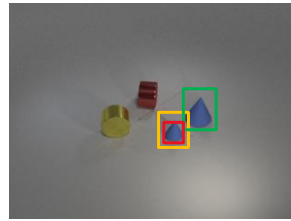
			
(<u>2</u> , <u>29</u> , <u>17</u>)	(<u>35</u> , <u>20</u> , <u>20</u>)	(<u>20</u> , <u>20</u> , <u>20</u>)	(<u>12</u> , <u>3</u> , <u>20</u>)
			
(<u>9</u> , <u>34</u> , <u>32</u>)	(<u>32</u> , <u>3</u> , <u>32</u>)	(<u>19</u> , <u>0</u> , <u>19</u>)	(<u>7</u> , <u>2</u> , <u>19</u>)
			
(<u>28</u> , <u>12</u> , <u>15</u> , <u>1</u>)	(<u>1</u> , <u>18</u> , <u>29</u> , <u>1</u>)	(<u>9</u> , <u>7</u> , <u>23</u> , <u>9</u>)	(<u>34</u> , <u>6</u> , <u>23</u> , <u>34</u>)
			
(<u>4</u> , <u>20</u> , <u>29</u> , <u>9</u>)	(<u>23</u> , <u>9</u> , <u>22</u> , <u>11</u>)	(<u>23</u> , <u>9</u> , <u>22</u> , <u>11</u>)	(<u>15</u> , <u>4</u> , <u>11</u> , <u>11</u>)
			
(<u>22</u> , <u>10</u> , <u>22</u>)	(<u>22</u> , <u>22</u> , <u>22</u>)	(<u>17</u> , <u>17</u> , <u>17</u>)	(<u>17</u> , <u>29</u> , <u>17</u>)

Table 12. Example rationales generated by our LRR model on CATER. The rationales contain the surrogate task of multi-target tracking. We show the predicted grid locations of the cones and the snitch below.